

High-Chromaticity Optics for the MAX IV 1.5 GeV Storage Ring

Teresia Olsson

May 26, 2014

MAX-lab Internal Note 20140526

Abstract

In case of instability issues during commissioning there might be a need for operating the MAX IV storage ring at a higher chromaticity than given by the design optics. The performance of an optics with linear chromaticity +4 in both transverse planes has been studied for the MAX IV 1.5 GeV storage ring. The possibility to operate such an optics in the real machine has also been examined. The studied high-chromaticity optics candidate was achieved by only brief optimization and by studying the performance of this optics the need for a more thorough optimization could be evaluated.

The performance of the studied candidate for high-chromaticity optics is considered good. No problems with the injection process are expected due to imperfections and the reduction of Touschek lifetime is small. The performance of the sextupole magnets in the MAX IV 1.5 GeV storage ring remains to be studied in detail, but it is expected that they should be able to produce the gradients required for the studied high-chromaticity optics, possibly with a substitution of power supplies. However, if in the future a more in-depth optimization of the high-chromaticity optics is desired the performance of the sextupole magnets has to be studied in greater detail to verify that they can produce the required gradients.

1 Introduction

In case of instability issues during commissioning there might be a need for operating the MAX IV storage rings at higher chromaticity than given by the design optics. Previously work a high-chromaticity optics for the MAX IV 3 GeV storage ring [1, 2] has been developed and the corresponding work has now been done for the MAX IV 1.5 GeV storage ring. The performance of an optics with linear chromaticity +4 in both transverse planes and the possibility to operate this optics in the real machine were studied.

2 Chromaticity Correction in the MAX IV 1.5 GeV Storage Ring

To make the lattice of the MAX IV 1.5 GeV storage ring more compact, the focusing sextupoles have been integrated into the focusing quadrupoles. The defocusing sextupoles are dedicated magnets and to allow adjustment of the chromaticity small focusing correction sextupoles have been inserted into the lattice. Since most of the focusing sextupole strength is implemented in iron it is only possible to adjust the chromaticity within a certain range depending on the gradients that the focusing correction sextupoles are able to produce [3].

The MAX IV 1.5 GeV storage ring has in total six sextupole families. The defocusing sextupole magnets are SDi and SDo, both dedicated sextupole magnet families. SDi is chromatic and SDo purely harmonic. The two main focusing sextupole families are SQFi and SQFo, where SQFi is chromatic and SQFo harmonic. These sextupoles are integrated into the quadrupole magnets and therefore their strength cannot be adjusted individually. To allow adjustment of the chromaticity two families of correction sextupoles have been added into the lattice, SCi and SCo. SCi is chromatic and SCo harmonic. These sextupoles are only used for small adjustments of the chromaticity and are therefore weak since the main chromaticity optimization is done by SQFi and SQFo [3].

The fixed sextupole strengths of SQFi and SQFo have been designed to correct the natural linear chromaticity of the lattice to +2 in both transverse planes and optimize the nonlinear behavior. This is the 531 nonlinear optics. The linear chromaticity has then been corrected to +1 in both planes using SCi and SDi. To improve the nonlinear dynamics, SCo has also been varied, while varying SDo was not required. This is the 533 nonlinear optics, hereafter referred to as the design optics [4].

3 MAX IV 1.5 GeV storage ring sextupole magnets

The sextupole magnets of the MAX IV 1.5 GeV storage ring have been designed to produce the gradients found in Table 1 [5]. A high-chromaticity optics requires other gradients and therefore the maximum gradients that the magnets are able to produce constrain the achievable performance of the high-chromaticity optics.

Table 1: Technical specification gradients for the MAX IV 1.5 GeV storage ring sextupole magnets [5].

Sextupole family	Technical specification gradients b_3 [m⁻³]
SDi	-74.1693
SDo	-102.061
SCi	-13.4646
SCo	-19.2266

4 Candidate for High-Chromaticity Optics

To study the performance of an optics with linear chromaticity +4 in both transverse planes, a candidate for high-chromaticity optics was developed. The candidate, named 534-1a, was achieved by correcting the linear chromaticities to +4 with SCi and SDi and then make small adjustments of the chromatic tune footprint with SCo and SDo to avoid the resonances assumed to be the most dangerous. By evaluating the performance of this optics the need for a more thorough optimization could be evaluated. The purpose of the high-chromaticity optics is to be used in case of instability issues during commissioning and therefore its performance should be sufficient to allow injection and machine studies. The requirements on the performance of the high-chromaticity optics is therefore not as stringent as for the design optics. The sextupole gradients of the 534-1a nonlinear optics can be found in Table 2.

Table 2: Sextupole gradients for the high-chromaticity optics.

Sextupole family	High- chromaticity optics b_3 [m⁻³]	Comp. to technical specification gradients [%]
SDi	-85.27	115%
SDo	-79.92	78%
SCi	13.028571	-97%
SCo	-8.00	42%

The correction of the chromaticities was done using OPA and the results were compared with results given by TRACY-3. This showed a small discrepancy in the chromaticities given by the two codes. Whereas OPA determined the linear chromaticity to +4.0 in both transverse planes, TRACY-3 found the horizontal linear chromaticity +3.422 and the vertical linear chromaticity +3.798 for the same optics. However, further analysis concluded that these differences were so small that they did not have any significant

effect on the results.

5 Tune Shifts

The chromatic tune shifts over the desired momentum acceptance $\pm 4\%$ are displayed in Fig. 1. The chromatic tune footprint is displayed in Fig. 2. The optimization of the chromatic tune footprint was focused on avoiding the $\nu_x + 2\nu_y = 18$ resonance.

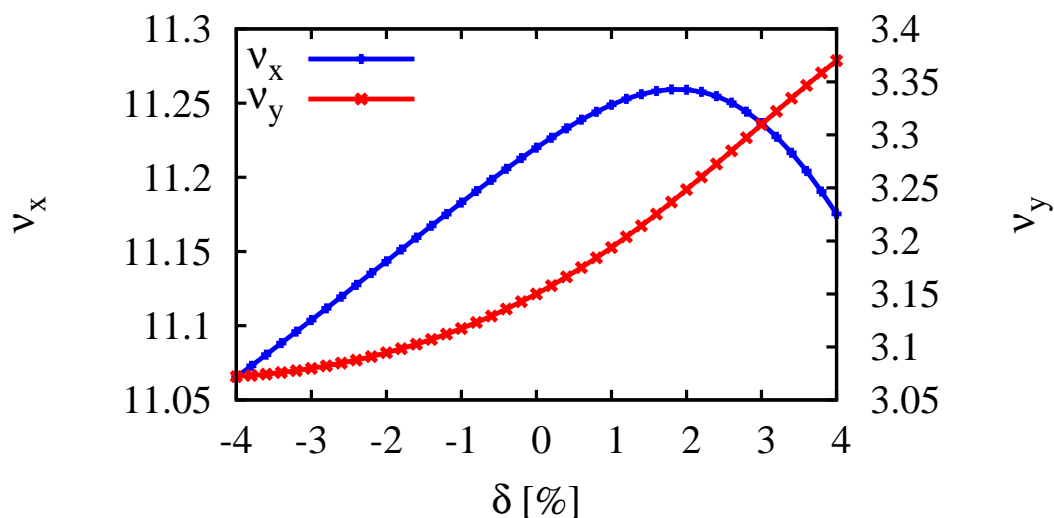


Figure 1: Chromatic tune shifts calculated with TRACY-3.

The amplitude-dependent tune shifts (ADTSs) over the required aperture, $x = 8.7\text{mm}$, $y = 4\text{ mm}$, are displayed in Fig. 3. The required aperture is in the horizontal plane given by the requirements for the injection process and in the vertical plane by constrains from insertion devices. To be able to study the performance of an optics with only brief optimization no optimization of the ADTSs were done. The ADTSs are therefore large.

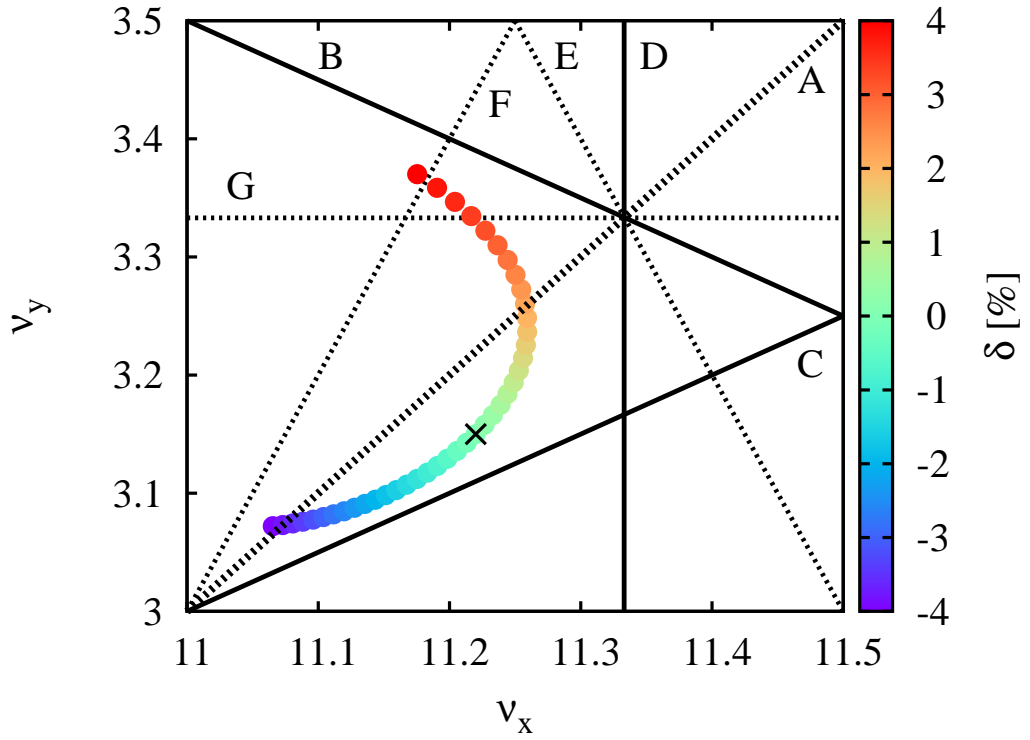


Figure 2: Chromatic tune footprint calculated with TRACY-3. The resonances up to third order are displayed. A: $\nu_x - \nu_y = 8$, B: $\nu_x + 2\nu_y = 18$, C: $\nu_x - 2\nu_y = 5$, D: $3\nu_x = 34$, E: $2\nu_x + \nu_y = 26$, F: $2\nu_x - \nu_y = 19$ and G: $3\nu_y = 10$. The working point is marked with a black cross.

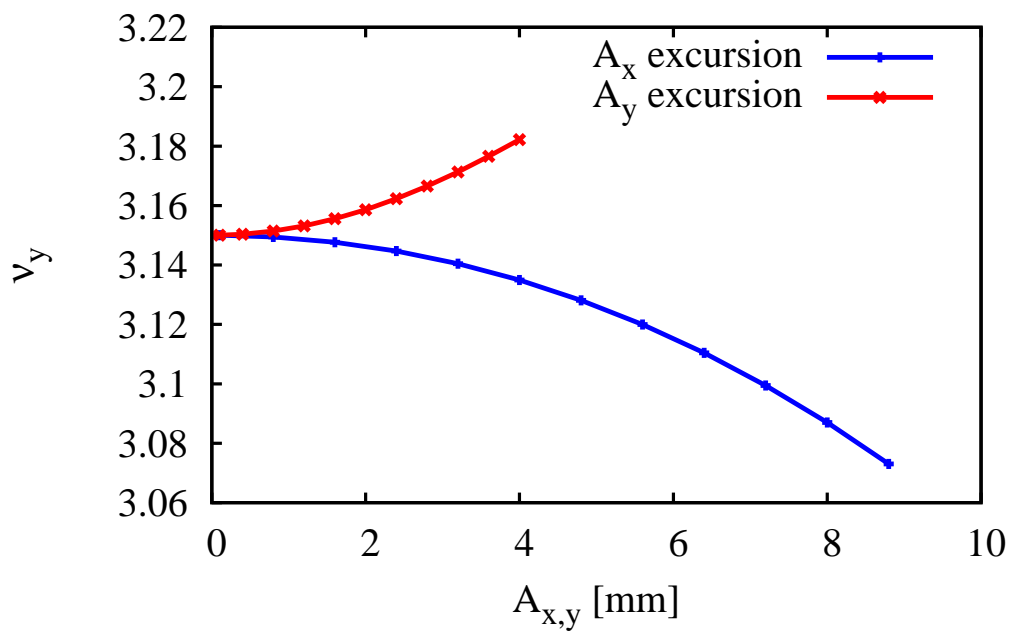
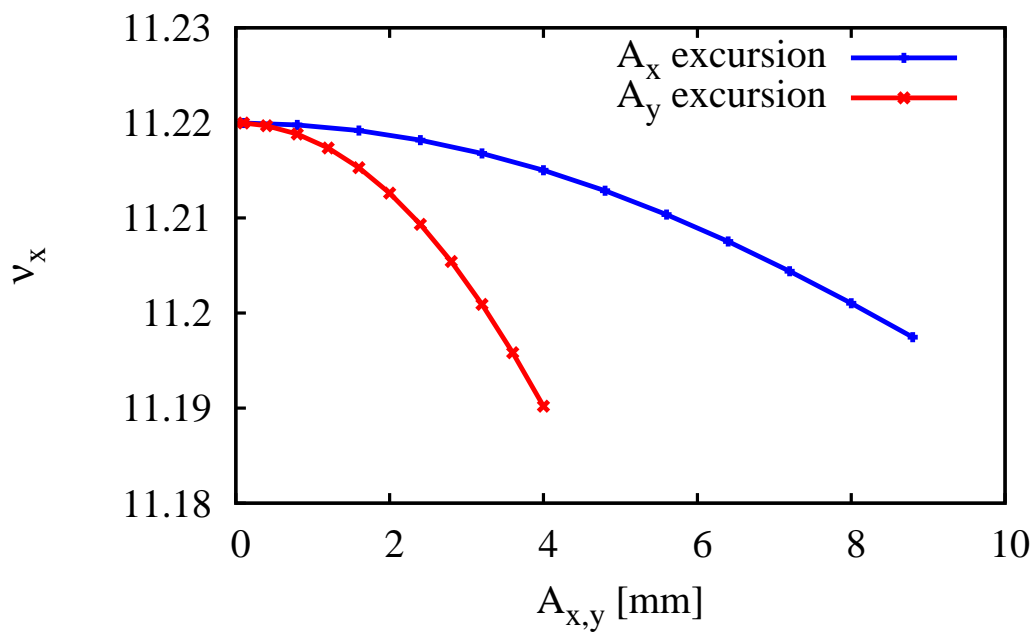


Figure 3: Amplitude-dependent tune shifts calculated with TRACY-3.

6 Dynamic Aperture

The dynamic aperture in the centre of the straight sections is displayed in Fig. 4. It is evident that the dynamic aperture without imperfections is larger than required both on and off-momentum. The on-momentum diffusion map is displayed in Fig. 5 and shows low diffusion inside the required aperture. A magnification of the diffusion map inside the physical aperture is displayed in Fig. 6 and the corresponding frequency map in Fig. 7. In the frequency map six resonances can be distinguished, $\nu_x - \nu_y = 8$, $\nu_x - 2\nu_y = 5$, $5\nu_x = 56$, $6\nu_x = 67$, $7\nu_x = 78$ and $7\nu_x - 2\nu_y = 72$, but comparison with the diffusion map shows that these have no significant effect inside the required aperture.

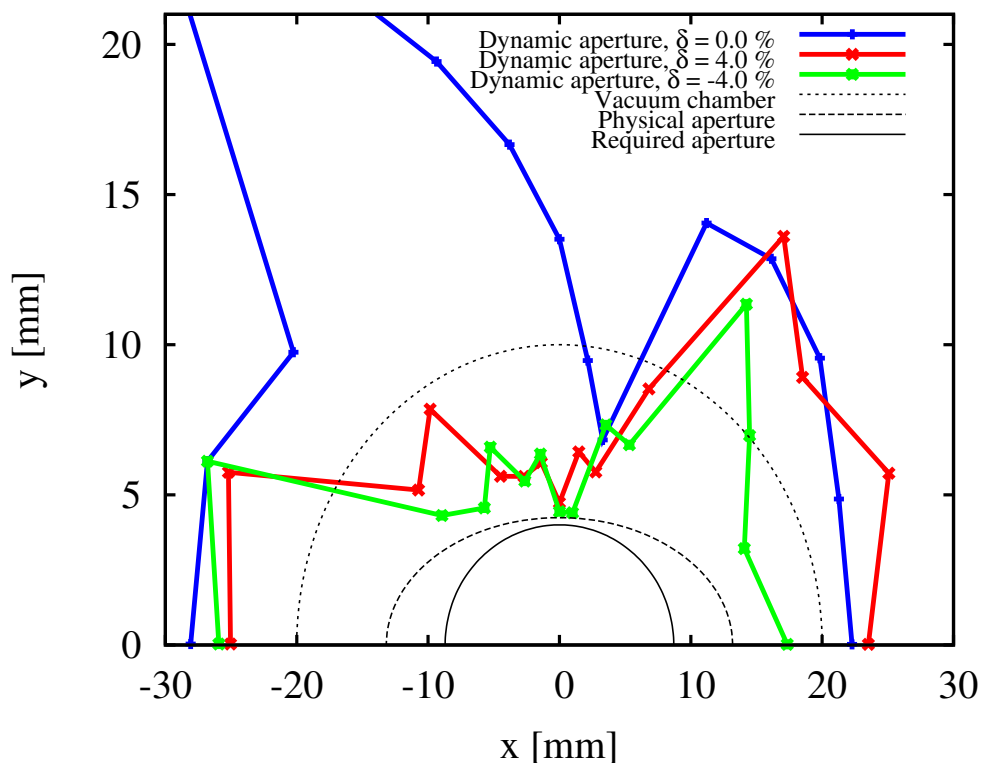


Figure 4: Dynamic aperture in the centre of the straight sections calculated with TRACY-3. The physical aperture is in the horizontal plane limited by the septum magnet used for injection and in the vertical plane by the aperture of the vacuum chamber.

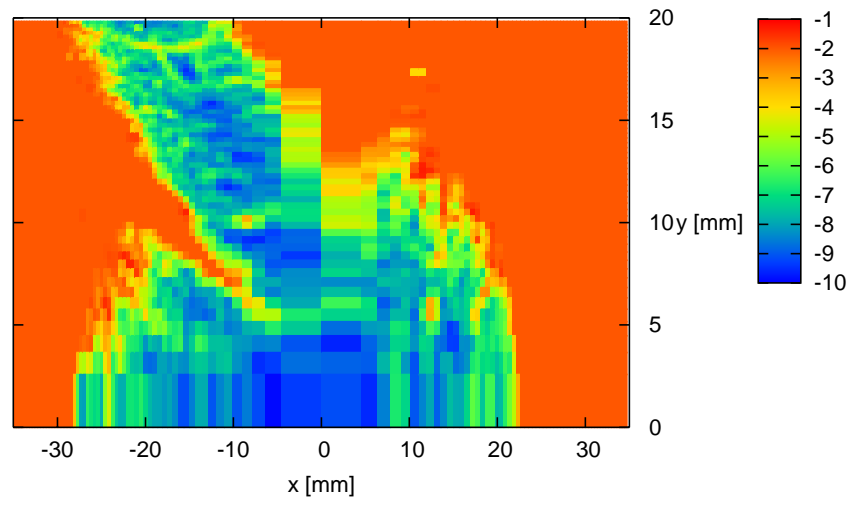


Figure 5: On-momentum diffusion map in the centre of the straight sections calculated with TRACY-3.

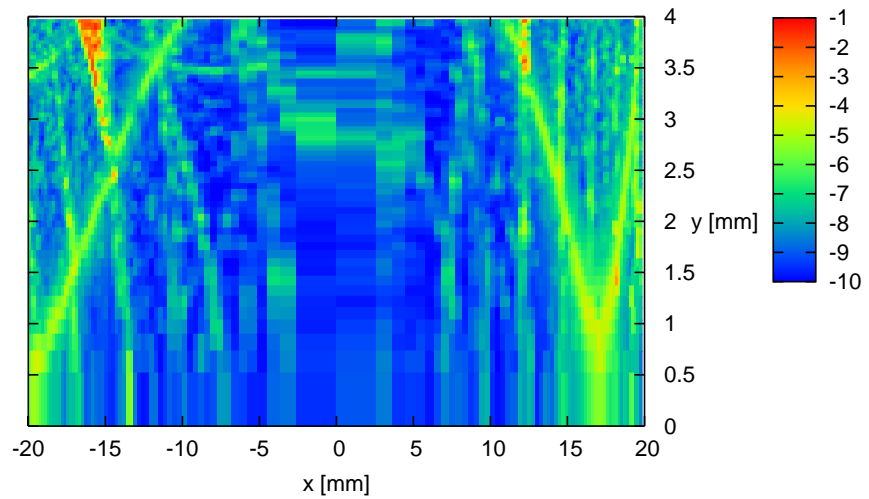


Figure 6: Magnification of the on-momentum diffusion map in the centre of the straight sections calculated with TRACY-3.

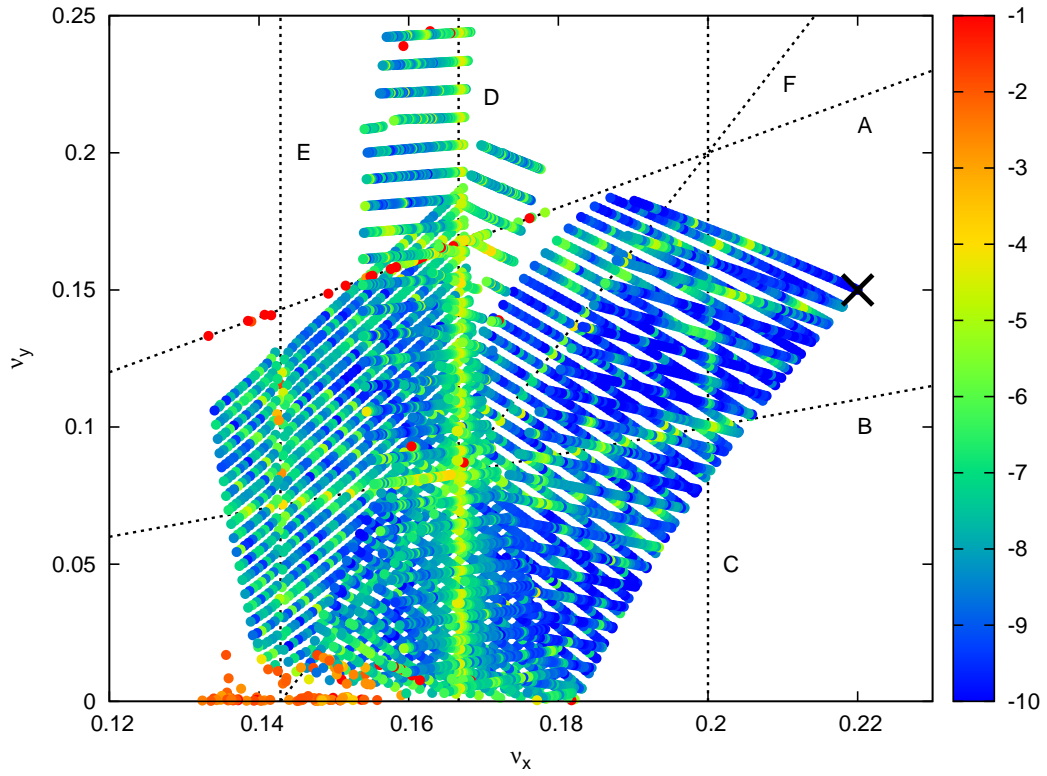


Figure 7: On-momentum frequency map in the centre of the straight sections calculated with TRACY-3. A: $\nu_x - \nu_y = 8$, B: $\nu_x - 2\nu_y = 5$, C: $5\nu_x = 56$, D: $6\nu_x = 67$, E: $7\nu_x = 78$ and F: $7\nu_x - 2\nu_y = 72$. The working point is marked with a black cross.

7 Momentum Acceptance

The off-momentum diffusion map is displayed in Fig. 8. A magnification of the diffusion map of over the desired momentum acceptance $\pm 4\%$ is displayed in Fig. 9 and the corresponding frequency map in Fig. 10. In the frequency map six resonances can be distinguished, $2\nu_x - \nu_y = 19$, $\nu_x - 2\nu_y = 5$, $4\nu_x = 45$, $4\nu_y = 13$, $6\nu_x = 67$ and $9\nu_x = 101$. The area with enlarged diffusion around $\delta = 1 - 3\%$ corresponds to $4\nu_x = 45$ and the area around $\delta = -1.5\%$ to $6\nu_x = 67$.

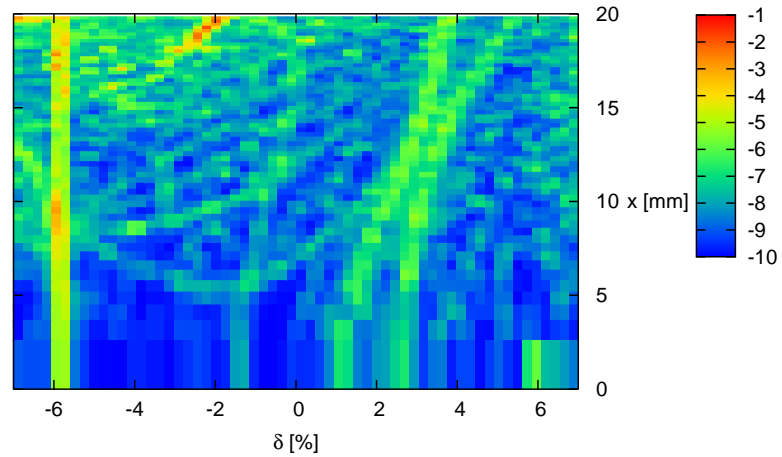


Figure 8: Off-momentum diffusion map in the centre of the straight sections calculated with TRACY-3.

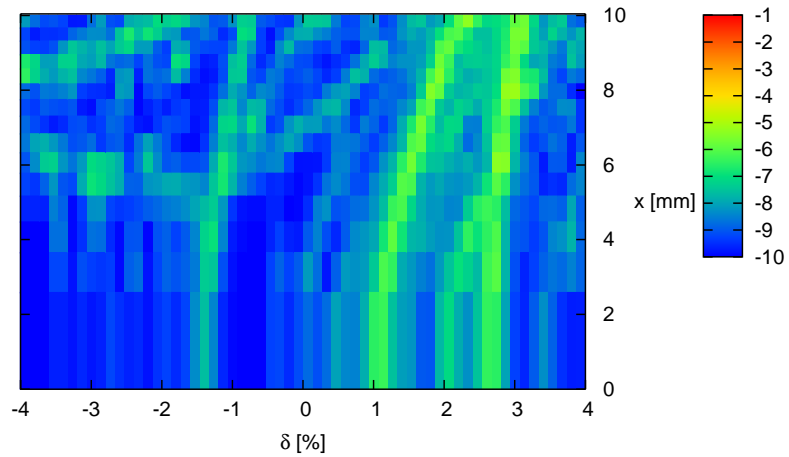


Figure 9: Magnification of the off-momentum diffusion map in the centre of the straight sections calculated with TRACY-3.

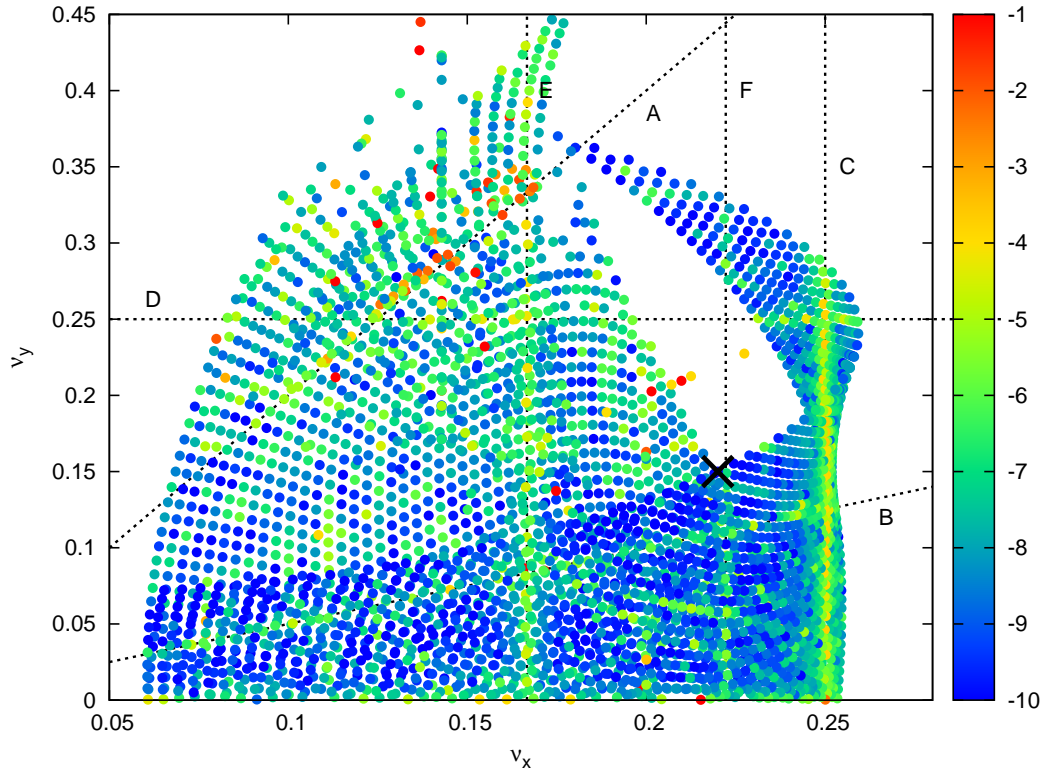


Figure 10: Off-momentum frequency map calculated with TRACY-3. A: $2\nu_x - \nu_y = 19$, B: $\nu_x - 2\nu_y = 5$, C: $4\nu_x = 45$, D: $4\nu_y = 13$, E: $6\nu_x = 67$ and F: $9\nu_x = 101$. The working point is marked with a black cross.

8 Error Model

8.1 Alterations to the Error Model

To study the performance of the real machine, errors were applied to the lattice. The error model used was based on the previous error model in [6], but some alterations of the model were done.

In accordance with [7] some modifications of the model were made to more closely model the orbit correction procedure in the real machine with TRACY-3. These modifications are explained in more detail in section 8.2. Also, the field and multipole errors were modified in accordance with [8], which are explained in more detail in section 8.3.

8.2 Alignment Errors

The following modifications of the error model were made:

- The girder definitions were removed so that all magnets as well as the BPMs would

be misaligned individually.

- The dipole slices forming an individual dipole magnet were placed onto a common girder and the individual misalignment of the slices was removed. Also SCi, SCo and the correctors were placed onto a common girder and their individual misalignments were removed. The girders were misaligned in both transverse planes by $25 \mu\text{m}$ rms and a roll error of 0.2 mrad rms. As previously in [6], this models the machining accuracy.
- The magnets adjacent to the BPMs, SQFi and SQFO, were misaligned by $3 \mu\text{m}$ rms in both transverse planes and a roll error of 0.2 mrad rms. Since the BPMs will be calibrated with respect to these magnets the transverse misalignments can be reduced to the level of the BPM calibration accuracy. However, the roll error was modeled with the same magnitude as the for the other magnets since the roll will not be calibrated directly together with the BPMs.

Apart from these modifications, the error model remained the same as in [6]. This means:

- SDi and SDo were misaligned according to the machine accuracy by $25 \mu\text{m}$ rms in both transverse planes and a roll error of 0.2 mrad rms.
- The calibration errors of the BPMs were assumed to be $3 \mu\text{m}$ rms in both transverse planes and a roll error of 0.1 mrad rms.

All the misalignments were modeled as a Gaussian distribution with a 2σ cut-off.

The dynamic aperture in the straight sections with alignment errors is displayed in Fig. 11. On-momentum the reduction of dynamic aperture due to misalignments occurs outside the vacuum aperture and therefore has no effect on the performance of the optics. Off-momentum the dynamic aperture reduction due to misalignments is larger for negative than for positive momentum deviations.

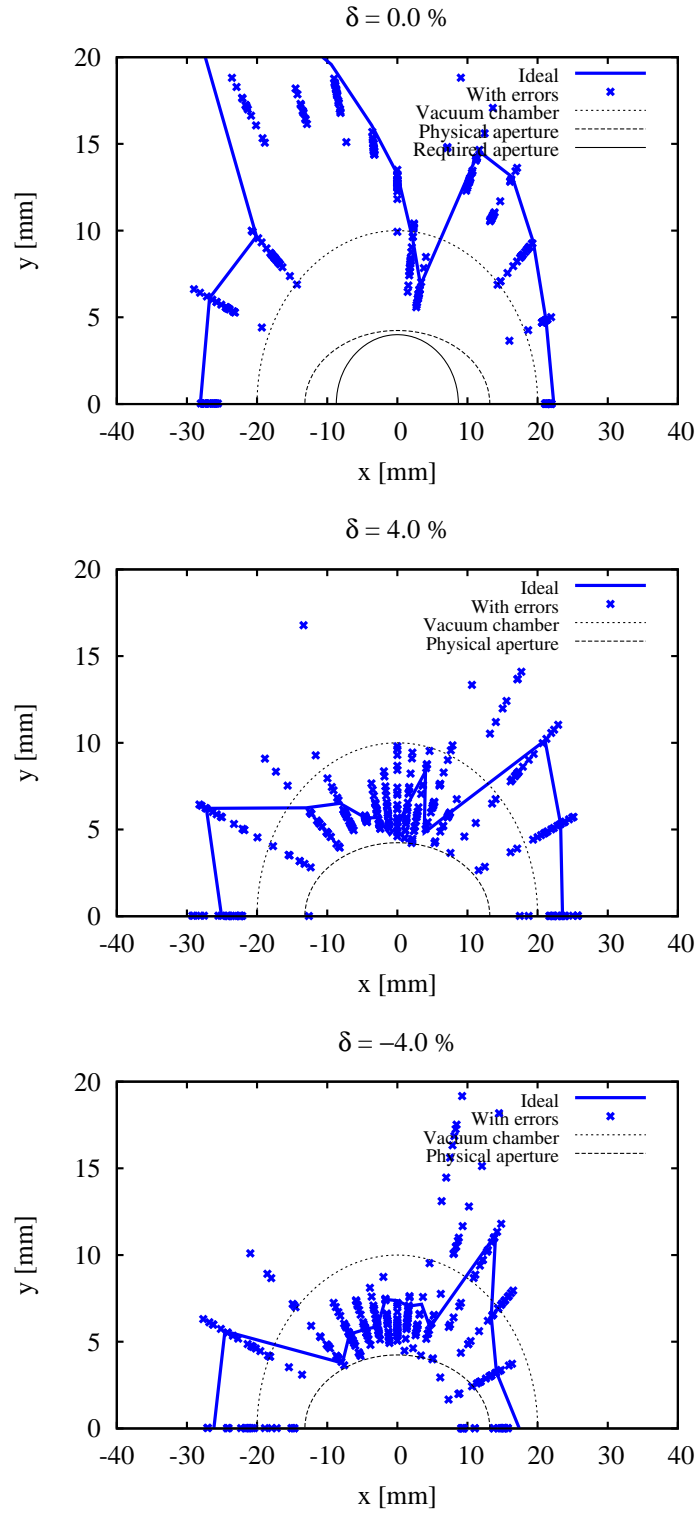


Figure 11: Dynamic aperture in the centre of the straight sections with alignment errors.

8.3 Field and Multipole Errors

The field errors in the magnets were modeled by applying a 0.05 % rms error to the following gradients:

- The quadrupole gradients in the dipole magnets.
- Both the quadrupole and the sextupole gradients in the quadrupole magnets.
- The sextupole gradients in the sextupole magnets.

To apply the errors with TRACY-3 the harmonic components were normalised with the radius of the good field region and the fundamental components as detailed in [9]. For the dipole slices the error was normalised according to a hard edge model of the entire dipole magnet. The errors were modeled as a Gaussian distribution with a 2σ cut-off. No systematic field errors were included in the error model.

The dynamic aperture with field errors is displayed in Fig. 12. It can be recognized that the reduction of dynamic aperture due to field errors is smaller than the reduction due to alignment errors.

The multipole errors were modeled as previously in [3] with measured magnets errors from the SLS storage ring [10]. The errors were rescaled according to the radius of the good field region for the MAX IV 1.5 GeV storage ring magnets and modelled as a Gaussian distribution with a 2σ cut-off. For harmonic components with both field and multipole errors the errors were added quadratically.

The dynamic aperture with field errors and multipole errors is displayed in Fig. 13. The reduction of dynamic aperture due to field and multipole errors are in the same order of magnitude as the reduction due to alignment errors, but the reduction in the horizontal plane is somewhat larger for the field and multipole errors. Still, the required aperture on-momentum is fulfilled.

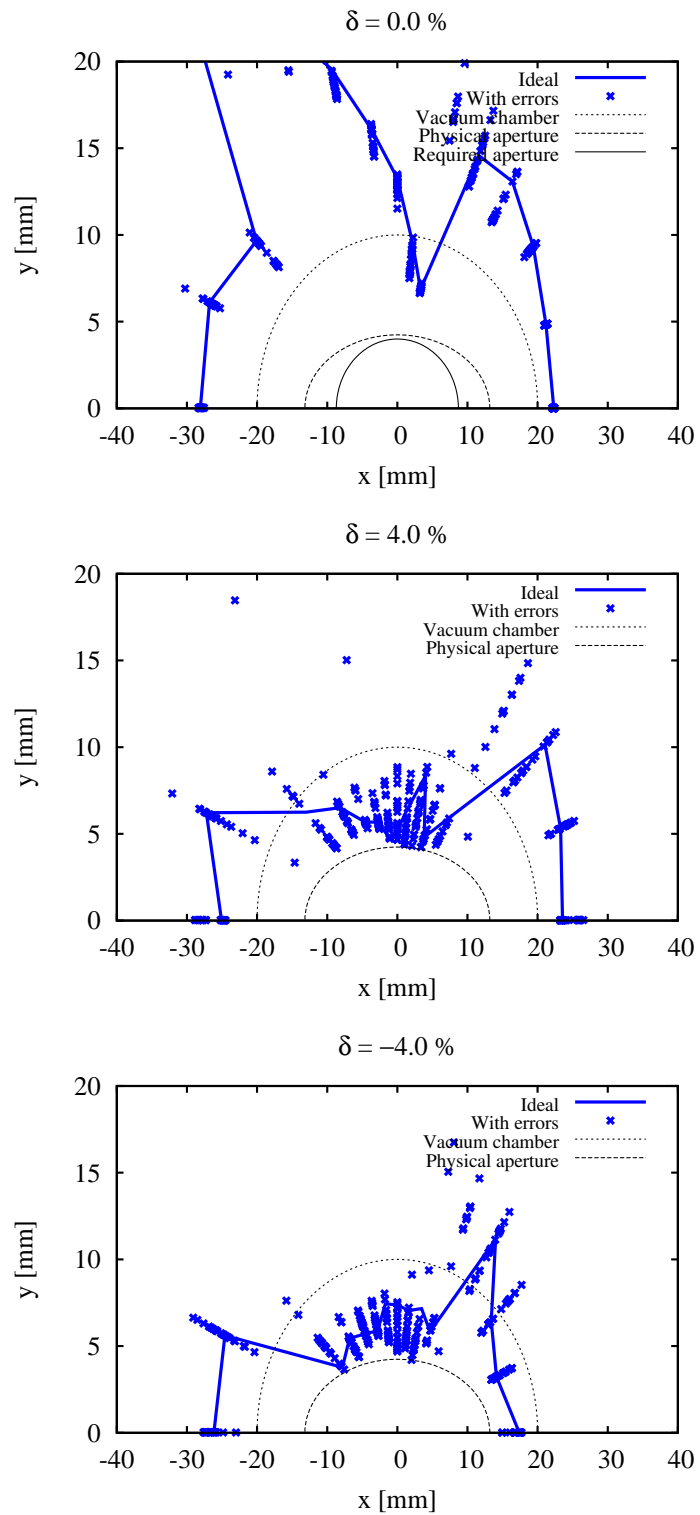


Figure 12: Dynamic aperture in the centre of the straight sections with field errors.

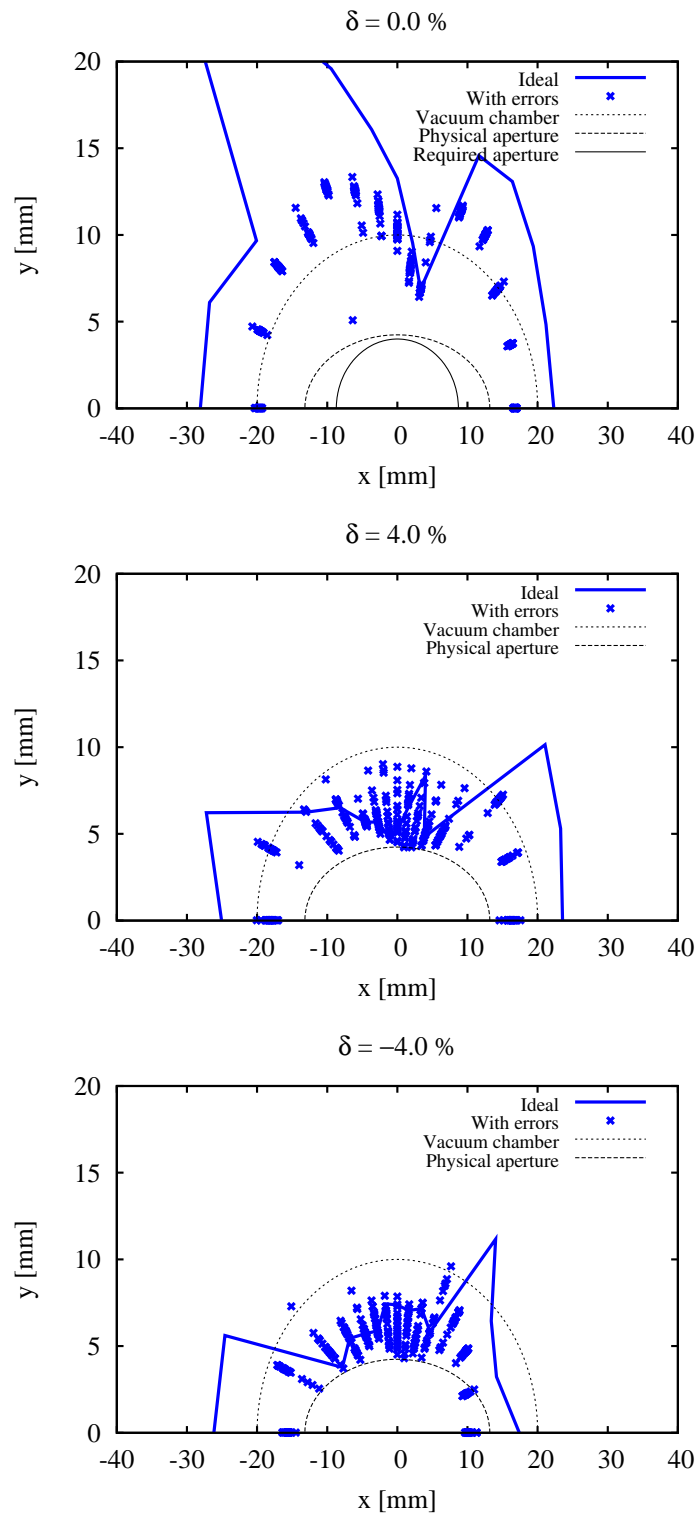


Figure 13: Dynamic aperture in the centre of the straight sections with field and multipole errors.

8.4 Effect of All Errors

The dynamic aperture with alignment, field and multipole errors is displayed in Fig. 14. On-momentum the reduction of dynamic aperture mostly takes place outside the vacuum aperture. The required aperture is still fulfilled and no problems with the injection process are therefore expected. Off-momentum the dynamic aperture reduction are larger for negative than for positive momentum deviations. However, the dynamic aperture reduction is not considered severe.

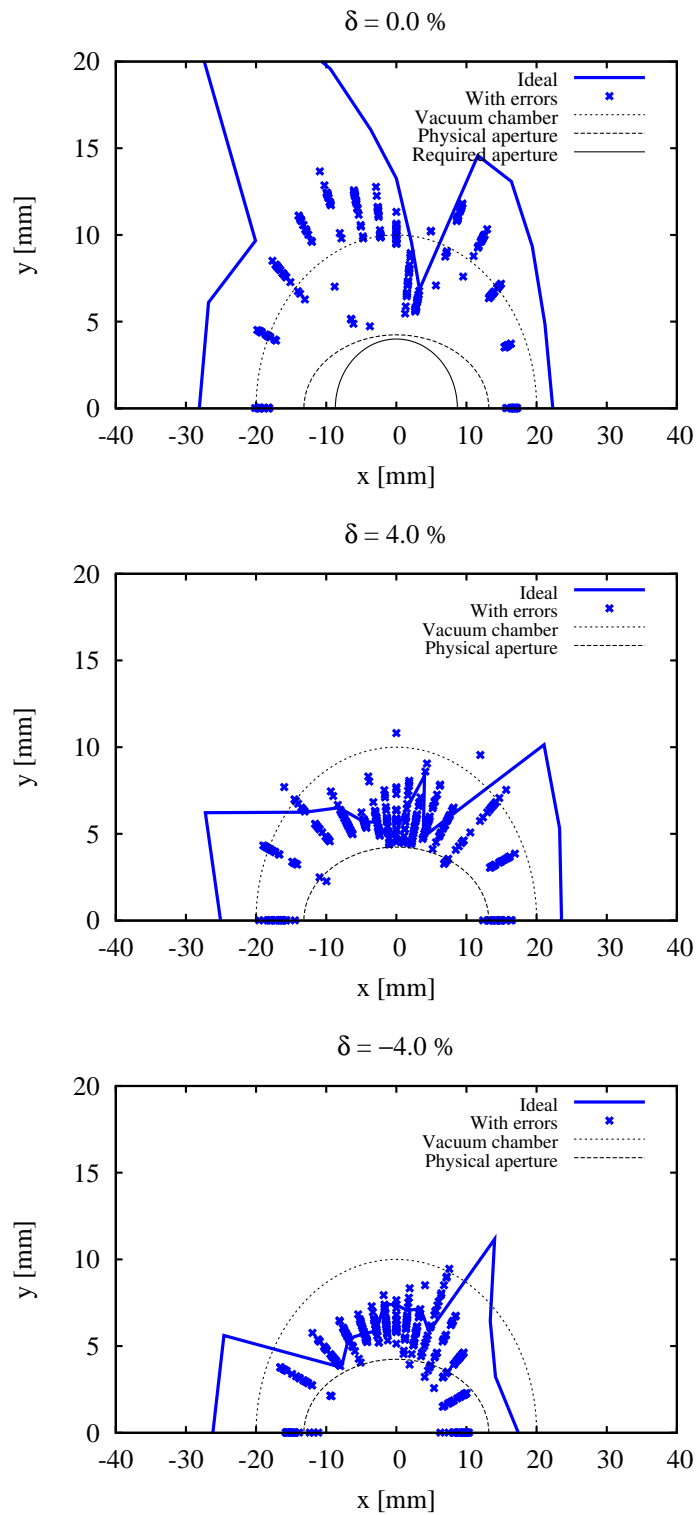


Figure 14: Dynamic aperture in the centre of the straight sections with alignment, field and multipole errors.

9 Touschek Lifetime

The Touschek lifetime without imperfections was calculated with 1 % coupling as 8.5 hours. The Touschek lifetime when all errors were applied to the lattice was calculated for 20 seeds. The coupling caused by the errors was calculated as 0.12 ± 0.1 % which responds to a Touschek lifetime of 2.6 ± 0.9 hours. This Touschek lifetime scaled to 1% coupling is 7.9 ± 0.4 hours. This is a reduction of roughly 7 %.

10 Conclusions

The performance of the studied candidate for high-chromaticity optics is considered good. No problems with the injection process due to imperfections are expected and the reduction of Touschek lifetime is small. Considering that the candidate was achieved with only brief optimization there exist possibilities to further increase the performance. However, the performance of the present candidate is sufficient to be able to apply the optics during commissioning.

The performance of the sextupole magnets in the MAX IV 1.5 GeV storage ring remains to be studied in detail, but it is expected that they should be able to produce the gradients needed for the studied high-chromaticity optics candidate. However, if in the future, a more in-depth optimization of the high-chromaticity optics is desired, the performance of the sextupole magnets has to be studied in more detail to verify that they can produce the required gradients.

References

- [1] T. Olsson, "High-chromaticity Optics for the MAX IV 3 GeV Storage Ring", Master's Thesis, October 2013, <http://www.eit.lth.se/srapport.php?uid=760>
- [2] T. Olsson, S.C Leemann, "High-chromaticity Optics for the MAX IV 3 GeV Storage Ring", TUPMA02, NA-PAC 2013, Pasadena, CA USA, <http://accelconf.web.cern.ch/AccelConf/PAC2013/papers/tupma02.pdf>
- [3] The MAX IV Detailed Design Report.
- [4] S.C. Leemann, "Updates to the MAX IV 1.5 GeV Storage Ring Lattice", MAX-lab Internal Note 20120904.
- [5] M. Johansson, "MAX IV 1.5 GeV Storage Ring Magnets - Technical Specification", 2012-06-07.
- [6] S.C. Leemann, "Updates to the MAX IV 1.5 GeV Storage Ring Lattice", MAX-lab Internal Note 20120313.
- [7] S.C. Leemann, "Alternative Orbit Correction Modeling for the MAX IV 3 GeV Storage Ring", MAX-lab Internal Note 20120724.

- [8] S.C. Leemann, "Updates to the MAX IV 3 GeV Storage Ring Lattice", MAX-lab Internal Note 20121107.
- [9] C.S Hwang et al. "Stretch-wire system for integral magnetic field measurements", Nuclear Instruments and Methods in Physics Research A 467-468 (2001) 194-197.
- [10] E.I Antokhin et al. "Precise Magnetic Measurements of the SLS Storage Ring Multipoles: Measuring System and Results, Proceedings of the Second Asian Particle Accelerator Conference, Beijing, China, 2001.